International Journal of Multiphase Flow 35 (2009) 628–639

Contents lists available at ScienceDirect

International Journal of Multiphase Flow

journal homepage: www.elsevier.com/locate/ijmulflow

Ensemble phase averaged equations for multiphase flows in porous media. Part 1: The bundle-of-tubes model

Dali Yang [a], Robert P. Currier [b], Duan Z. Zhang [c,*]

[a] Polymers and Coatings Group, Material Science and Technology Division, MST-7, MS E549, Los Alamos National Laboratory, Los Alamos, NM 87545, USA
[b] Physical Chemistry and Applied Spectroscopy Group, Chemistry Division, C-PCS, MS J567, Los Alamos National Laboratory, Los Alamos, NM 87545, USA
[c] Fluid Dynamics and Solid Mechanics Group, Theoretical Division, T-3, MS B216, Los Alamos National Laboratory, Los Alamos, NM 87545, USA

ARTICLE INFO

Article history:
Received 18 February 2009
Received in revised form 28 February 2009
Accepted 11 March 2009
Available online 19 March 2009

Keywords:
Porous media
Multiphase flow
Ensemble phase average

ABSTRACT

A bundle-of-tubes construct is used as a model system to study ensemble averaged equations for multiphase flow in a porous material. Momentum equations for the fluid phases obtained from the method are similar to Darcy's law, but with additional terms. We study properties of the additional terms, and the conditions under which the averaged equations can be approximated by the diffusion model or the extended Darcy's law as often used in models for multiphase flows in porous media. Although the bundle-of-tubes model is perhaps the simplest model for a porous material, the ensemble averaged equation technique developed in this paper assumes the very same form in more general treatments described in Part 2 of the present work (Zhang, D.Z., 2009. Ensemble Phase Averaged Equations for Multiphase Flows in Porous Media, Part 2: A General Theory. Int. J. Multiphase Flow 35, 640–649). Any model equation system intended for the more general cases must be understood and tested first using simple models. The concept of ensemble phase averaging is dissected here in physical terms, without involved mathematics through its application to the idealized bundle-of-tubes model for multiphase flow in porous media.

1. Introduction

Flow of immiscible fluids in various porous materials is of special importance to soil science, chemical, environmental, construction, and petroleum industries. In these systems, capillary action plays a crucial role in driving the motion of fluids within the porous media (Washburn, 1921; Richards, 1931; Scheidegger, 1974; Ianson and Hoff, 1986; Hall et al., 1984; Gray and Hassanizadeh, 1991; Liu, 1991; Hassanizadeh and Gray, 1993; Alava et al., 2004; Faybishenko, 2004). Extensive theoretical investigations and advanced experimental techniques, such as neutron radiography, have been applied to study the motion of the fluids (Gummerson et al., 1979; Hassanizadeh and Gray, 1993; Moseley and Dhir, 1996; Beliaev and Hassanizadeh, 2001; Gray et al., 2002; Lockington and Parlange, 2003; Tsakiroglou et al., 2003; Culligan et al., 2004; Shiozawa and Fujimaki, 2004; El Abd et al., 2005; Manthey et al., 2005; Le Guen and Kovscek, 2006; Hilfer, 2006; Czachor, 2007; Hall, 2007). Despite intensive interrogation, models for such flows are still largely empirical. Typically, the motion of fluids in a porous material are assumed either to be nonlinear diffusion processes (Lockington and Parlange, 2003; Pachepsky et al., 2003; El Abd et al., 2005), or to obey the same Darcy's law as in a single phase flow (Richards, 1931; Brooks and Corey, 1964). The diffusion approach is based on the early work of Washburn (1921). This approach is mainly used to model liquid imbibition in porous solids. The main focus for this model is liquid motion, while the motion of the other fluid, typically a gas, is not emphasized. In this paper we explain the reason why the diffusion approach is more successful in liquid-gas systems than in liquid-liquid systems. In the Darcy's law approach, each fluid in the porous material is driven by the pressure gradient. The application of Darcy's law to multiphase flows in porous materials is a significant extension of Darcy's law originally developed for a single phase flow in porous materials. For the cases of two-phase flow, this extension requires a closure model to describe the pressure difference between phases. The pressure difference is usually taken to be the capillary pressure (Leverett, 1941) with an implicit assumption that the pressure difference is caused solely by the interfacial surface tension between fluids. In liquid-gas two-phase flows, it was originally thought that the pressure difference was only a function of the liquid saturation. Later, experimental observations found that the pressure difference exhibits more complicated characters. The validity of both the diffusion approach and extensions of Darcy's law have been questioned (Gummerson et al., 1979; Hillel, 1980; Hassanizadeh and Gray, 1993; Prat, 1995; Lockington and Parlange, 2003; Tsakiroglou et al., 2003; Shiozawa and Fujimaki, 2004; Hilfer, 2006; Le Guen and Kovscek, 2006; Czachor, 2007; DiCarlo, 2007; Hall, 2007).

To develop equations describing the motion of fluids in porous materials, the multiphase flows in a porous material are treated as special cases of multi-material interactions involving

* Corresponding author. Tel.: +1 505 665 4428; fax: +1 505 665 5926.
E-mail address: dzhang@lanl.gov (D.Z. Zhang).

0301-9322/$ - see front matter © 2009 Elsevier Ltd. All rights reserved.
doi:10.1016/j.ijmultiphaseflow.2009.03.002

two fluid phases and one porous solid phase using ensemble phase averaging method (Zhang et al., 2007; Zhang, 2009). The closure relations associated with the averaged equations are expressed as averages of the interactions on phase interfaces. The averaged equations derived this way are in a form similar to the extended Darcy's law, but with additional terms. The presentation of this work is divided into two parts appearing as separate papers in this Journal. In Part 1, we illustrate the ensemble phase averaging method using a simple but meaningful example. General theory for multiphase flows in porous material is described in Part 2 (Zhang, 2009).

This paper is Part 1, in which we apply the ensemble averaging method to a bundle-of-tubes model for two-phase flows in porous materials. The main objective of this paper is to understand the additional terms that arise in the averaged equations, and to study their properties and the possible closure of the equations using this simple example. Although a typical porous material has a much more complex morphology than that captured by the bundle-of-tubes model, the model does possess a unique advantage of being conceptually simple and amenable to analytical solution. This porous material model has been used by Dahle et al. (2005) to study the behavior of the capillary pressure. By using the bundle-of-tubes model, we hope to explain the physical meaning of the closure relationships.

We will show that, despite of its simplicity, dissecting the averaged equations associated with the bundle-of-tubes model provides interesting insight into characteristics common to more complex porous materials. From the point view of the averaged equations, any theoretical model intended for describing two-phase flows should first be validated in a simple system such as this. The study of this simple bundle-of-tubes provides a starting point to study more general cases described in Part 2 of the present work.

2. Flow in capillary tubes

We consider a one-dimensional two-phase flow in a porous material consisting of parallel capillary tubes with various diameters as shown in Fig. 1. Let L be the length of the capillary tubes, ϕ be the diameters of the capillary tube, and β be the contact angle of fluid 1 on the solid wall, measured from the solid wall in contact with fluid 1 to the interface between fluids 1 and 2. For capillary tubes, the curvature radius a of the fluid interface can be calculated as $a = \phi/(2\cos\beta)$. In this example, we suppose that there is a reservoir of fluid 1 on the left of the capillary tubes. Initially the capillary tubes are filled with fluid 2 and are connected to a reservoir of fluid 2 on the right ends. Let p_L and p_R denote the pressures in left and right reservoirs, respectively, as illustrated in Fig. 1. Inside a given capillary tube the flow is a Poiseuille flow, except for in the region close to the interface between two phases. The momentum equations can be written as

$$\frac{32\mu_1}{\phi^2}\bar{u}_1 = -\nabla p_1 = \frac{p_L - p_1(x_I)}{x_I}, \quad x < x_I \tag{1}$$

and

$$\frac{32\mu_2}{\phi^2}\bar{u}_2 = -\nabla p_2 = \frac{p_2(x_I) - p_R}{L - x_I}, \quad x > x_I, \tag{2}$$

where μ_1 and μ_2 are viscosities, $\bar{u}_1$ and $\bar{u}_2$ are velocities of fluids 1 and 2 averaged over the tube cross section, $p_1(x)$ and $p_2(x)$ are pressures for fluids 1 and 2 within the tube, x_I is the interface location as measured from the left end of the capillary tube. Because of the curvature of the fluid interface in a capillary tube, the interface location can only be determined within an error of order of the diameter of the tube. In this example we assume that the length of the tube is much greater than the tube diameter, $L \gg \phi$. As a consequence of this assumption, an error of order ϕ/L is expected in the quantities calculated in this paper. In formulating the equations above we have used the fact that the diameter of a tube is independent of location x, and the pressures vary linearly in a tube within a given fluid. Across the fluid interface, the pressure difference caused by surface tension is

$$p_2(x_I) - p_1(x_I) = 2\Gamma_{21}/a = 4\Gamma_{21}\cos\beta/\phi. \tag{3}$$

Continuity of the fluid phases requires $\bar{u}_1 = \bar{u}_2$ in a capillary tube. Using this relation, we can eliminate the pressures p_1 and p_2 at the interface from (1) and (2), and find

$$\bar{u}_1 = \bar{u}_2 = \frac{\phi^2\Delta p + 4\Gamma_{21}\phi\cos\beta}{32\mu_1 x_I + 32\mu_2(L - x_I)}, \tag{4}$$

where $\Delta p = p_L - p_R$ is the pressure difference between the reservoirs at the ends of the capillary tubes.

For simplicity, we assume $\Delta p \geqslant 0$ and $\Gamma_{21} \geqslant 0$, hence the velocity of the invading fluid 1 increases with the capillary diameter. The interface location can be calculated by solving $dx_I/dt = \bar{u}_1$. The solution is

$$\phi(\phi\Delta p + 4\Gamma_{21}\cos\beta)t = 16\mu_1 x_I^2 + 16\mu_2(2Lx_I - x_I^2). \tag{5}$$

This solution relates the penetration of fluid 1 to the diameter of the capillary tube. Given a fluid interfacial position x and time t, we can use (5) to find a diameter $\phi(x, t)$ of the tubes that the fluid interfaces are in. For a capillary tube with a specified diameter ϕ, one can also use (5) to find the location of the fluid interface in the tube, $x_I(\phi, t)$. The interface location $x_I(\phi, t)$ is an increasing function of ϕ. The pressure within a capillary tube is found by substituting (4) into Eqs. (1) and (2)

$$p_1(x, t, \phi) = p_L - \frac{\mu_1(\Delta p + 4\Gamma_{21}\cos\beta/\phi)x}{\mu_1 x_I(\phi, t) + \mu_2[L - x_I(\phi, t)]}, \quad x < x_I \tag{6}$$

and

$$p_2(x, t, \phi) = p_R + \frac{\mu_2(\Delta p + 4\Gamma_{21}\cos\beta/\phi)(L - x)}{\mu_1 x_I(\phi, t) + \mu_2[L - x_I(\phi, t)]}, \quad x > x_I. \tag{7}$$

These results are obtained based on the Poiesuille flow in a circular capillary tube. Near a fluid interface the flow is not a true Poiesuille flow and the pressures are different. The size of the region where the pressures differ significantly is of the order of the diameter of the capillary tube. When pressures derived from (6) and (7) are used to calculate the average pressures, or the phase interaction forces, an error of order ϕ/L should be expected.

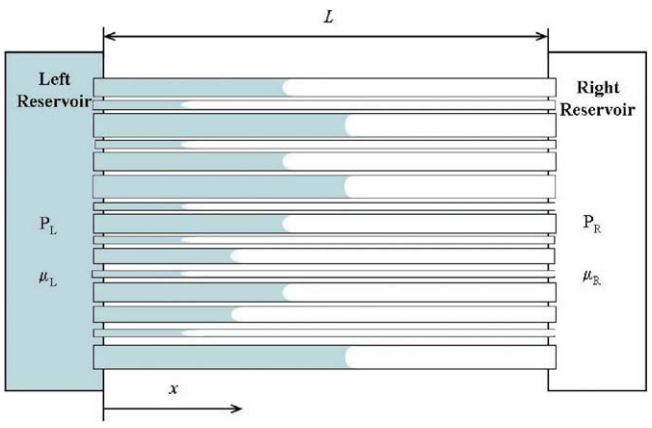

Fig. 1. The illustration of ensemble of capillaries with different diameters.

3. Ensemble phase averaged equations

With the analytical solutions for pressures and velocities listed above, we can apply the ensemble phase averaging method to study properties of the resulting closure quantities in this simple geometry. The ensemble phase averaging method has been used previously to derive averaged equations for disperse multiphase flows (Zhang and Prosperetti, 1994, 1997). The method has also been extended for continuous multiphase flows with infinite number of degrees of freedom in the system (Zhang et al., 2007). In the ensemble phase averaging method, at a given location $\boldsymbol{x}$ and time t, the average of a quantity pertaining to a specified phase is calculated by averaging over all the flow realizations in which the specified location is occupied by that phase at the time. Although a general derivation of the averaged equations has been developed in Part 2 of this work (Zhang, 2009), for the simple bundle-of-tubes geometry the derivation of the ensemble phase averaged equations can be significantly simplified. This simplified derivation illustrates the physical interactions on the phase interfaces with much fewer mathematical steps. In this section we present this derivation. For general derivations, readers are referred to the cited work (Zhang et al., 2007; Zhang, 2009).

In the ensemble averaging method, the volume fraction θ_1 of fluid 1 at any point is calculated as the probability of the point occupied by the fluid. In the simple bundle-of-tubes model, this probability can be calculated geometrically as the ratio of the cross section area of the capillary tubes containing fluid 1 to the total area, A_T, of the cross section. Let N_T be the total number of tubes in the cross section and $P(\phi)$ be the probability distribution of the tube diameters. For a specified location x and time t, the penetration depth of the invading fluid increases with the diameter of the tube. Thus fluid 1 will only occupy capillary tubes with a diameter larger than the $\phi(x,t)$ calculated from (5) by replacing x_I with x. The respective areas occupied by fluids 1 and 2 in the cross section are

$$A_1 = N_T \int_{\phi(x,t)}^{\infty} \frac{\pi\phi^2}{4} P(\phi)\, d\phi, \quad A_2 = N_T \int_0^{\phi(x,t)} \frac{\pi\phi^2}{4} P(\phi)\, d\phi, \tag{8}$$

and their volume fractions of fluids 1 and 2 can be calculated as $\theta_i(x,t) = A_i/A_T$, or

$$\theta_1(x,t) = n_A \int_{\phi(x,t)}^{\infty} \frac{\pi\phi^2}{4} P(\phi)\, d\phi, \quad \theta_2(x,t) = n_A \int_0^{\phi(x,t)} \frac{\pi\phi^2}{4} P(\phi)\, d\phi, \tag{9}$$

where $n_A = N_T/A_T$ is the number of the tubes per unit cross section area. The gradient of the volume fractions can be calculated as

$$\nabla\theta_1(x,t) = -\nabla\theta_2(x,t) = -n_A \frac{\pi\phi^2}{4} P(\phi) \frac{\partial\phi(x,t)}{\partial x}. \tag{10}$$

The degree of saturation for fluid i can be defined as $S_i = \theta_i/(\theta_1 + \theta_2)$ for $i = 1, 2$. Then,

$$S_1(x,t) = \int_{\phi(x,t)}^{\infty} \phi^2 P(\phi)\, d\phi \Big/ \int_0^{\infty} \phi^2 P(\phi)\, d\phi,$$
$$S_2(x,t) = \int_0^{\phi(x,t)} \phi^2 P(\phi)\, d\phi \Big/ \int_0^{\infty} \phi^2 P(\phi)\, d\phi. \tag{11}$$

For a given position and time, the average of a quantity pertaining to a phase is then calculated by averaging over all possible values of that quantity for which the spatial position of interest is occupied by the phase at the specified time. In this bundle-of-tubes model, the chance of a tube being selected as a sample is proportional to its cross section area. Hence in this example, the ensemble phase average of a quantity becomes a cross section area weighted average. Again, since the invading fluid only occupies the tubes with diameter greater than $\phi(x,t)$, the average pressure $\langle p_1\rangle$, the average pressure gradient, and the average velocity $\langle u_1\rangle$ can be calculated as

$$\langle p_1\rangle = \int_{\phi(x,t)}^{\infty} \frac{\pi\phi^2}{4} p_1(x,t,\phi) P(\phi)\, d\phi \Big/ \int_{\phi(x,t)}^{\infty} \frac{\pi\phi^2}{4} P(\phi)\, d\phi, \tag{12}$$

$$\langle \nabla p_1\rangle = \int_{\phi(x,t)}^{\infty} \frac{\pi\phi^2}{4} \nabla p_1(x,t,\phi) P(\phi)\, d\phi \Big/ \int_{\phi(x,t)}^{\infty} \frac{\pi\phi^2}{4} P(\phi)\, d\phi, \tag{13}$$

$$\langle u_1\rangle = \int_{\phi(x,t)}^{\infty} \frac{\pi\phi^2}{4} \bar{u}_1(x,t,\phi) P(\phi)\, d\phi \Big/ \int_{\phi(x,t)}^{\infty} \frac{\pi\phi^2}{4} P(\phi)\, d\phi. \tag{14}$$

Similarly the receding fluid occupies the tubes with the diameter less than $\phi(x,t)$, the cross section area weighted averages for the pressure, the pressure gradient and the velocity are given by

$$\langle p_2\rangle = \int_0^{\phi(x,t)} \frac{\pi\phi^2}{4} p_2(x,t,\phi) P(\phi)\, d\phi \Big/ \int_0^{\phi(x,t)} \frac{\pi\phi^2}{4} P(\phi)\, d\phi, \tag{15}$$

$$\langle \nabla p_2\rangle = \int_0^{\phi(x,t)} \frac{\pi\phi^2}{4} \nabla p_2(x,t,\phi) P(\phi)\, d\phi \Big/ \int_0^{\phi(x,t)} \frac{\pi\phi^2}{4} P(\phi)\, d\phi, \tag{16}$$

$$\langle u_2\rangle = \int_0^{\phi(x,t)} \frac{\pi\phi^2}{4} \bar{u}_1(x,t,\phi) P(\phi)\, d\phi \Big/ \int_0^{\phi(x,t)} \frac{\pi\phi^2}{4} P(\phi)\, d\phi. \tag{17}$$

The volume fractions and averages defined above, can be used to derive averaged equations. Using (9), we find

$$\theta_1(x,t)\langle p_1\rangle(x,t) = n_A \int_{\phi(x,t)}^{\infty} \frac{\pi\phi^2}{4} p_1(x,t,\phi) P(\phi)\, d\phi, \tag{18}$$

where we employ the notation $\langle p_1\rangle(x,t) = \langle p_1(x,t,\phi)\rangle$. Upon differentiation of (18) with respect to x, and using (9), (10), (12), and (13), we find

$$\theta_1 \nabla\langle p_1\rangle = \theta_1 \langle \nabla p_1\rangle + [\langle p_1\rangle_I - \langle p_1\rangle] \nabla\theta_1, \tag{19}$$

where $\langle p_1\rangle_I = p_1(x,t,\phi(x,t))$ is the pressure of fluid 1 on the phase interface with fluid 2. The gradient $\nabla\langle p_1\rangle$ can be viewed as the slope of the increase in the average pressure from location x to location $x + \Delta x$ for an infinitesimal Δx. The average pressure $\langle p_1\rangle(x,t)$ is calculated by averaging over the pressures in the tubes in which the point x is occupied by fluid 1 at time t. Since fluid 1 occupies different sets of tubes in location x and $x + \Delta x$, the average pressures $\langle p_1\rangle(x + \Delta x, t)$ and $\langle p_1\rangle(x,t)$ are calculated using the pressures taken from different sets of tubes. As the location changes from x to $x + \Delta x$ the set of tubes used to calculate the average pressure may gain additional tubes or lose tubes. If the pressure p_1 in the gained or lost tubes is greater than the average pressure $\langle p_1\rangle$, (i.e. $p_1 - \langle p_1\rangle > 0$), then the process of gaining the tubes increases the average pressure $\langle p_1\rangle$; and the process of losing tubes decreases the average pressure. In the gained tubes, $x + \Delta x$ is in fluid 1 but not x. Similarly, in the lost tubes, x is in fluid 1 but not $x + \Delta x$. Since Δx is infinitesimal, in these gained or lost tubes x can be regarded on the interface between the fluids; and then p_1 is the pressure on the fluid interface. This change in the set of the tubes occupied by fluid 1 is represented by the volume fraction gradient $\nabla\theta_1$. The last term of (19) accounts for this contribution to the average pressure increase due to the pressure difference $\langle p_1\rangle_I - \langle p_1\rangle$ on the phase interface and the volume fraction gradient $\nabla\theta_1$ representing the change of the tube sets from x to $x + \Delta x$. The first term on the right hand side of (19) accounts for the average pressure increase due to the pressure change inside fluid 1 itself. Relation (19) implies that in the ensemble phase

averaging method, the average operator and the differentiation operator do not commute. To commute them a term

$$F_{12} = [\langle p_1\rangle_I - \langle p_1\rangle]\nabla\theta_1 \tag{20}$$

is needed in (19).

Averaging over the momentum equation (1) and then using (19), we obtain

$$n_A \int_{\phi(x,t)}^{\infty} 8\mu_1\pi\bar{u}_1 P(\phi)\,d\phi = -\theta_1\langle\nabla p_1\rangle = -\theta_1\nabla\langle p_1\rangle + F_{12}. \tag{21}$$

Averaged momentum equation (21) shows that the flow in a porous media is driven by the average of the pressure gradient $\langle\nabla p_1\rangle$, not by the gradient $\nabla\langle p_1\rangle$ of the average pressure as in the extended Darcy's law for multiphase flows. Since these two quantities are different, but related by (19), the term F_{12} is needed to correct the extended Darcy's law.

The left hand side of Eq. (21) represents the viscous drag acting on fluid 1. If we write the viscous drag on the left hand side of (21) as $\theta_1 C_{1s}\mu_1\langle u_1\rangle$ then the drag coefficient can be calculated as

$$C_{1s} = \int_{\phi(x,t)}^{\infty} 32\bar{u}_1 P(\phi)\,d\phi \Big/ \int_{\phi(x,t)}^{\infty} \phi^2\bar{u}_1(x,t,\phi)P(\phi)\,d\phi. \tag{22}$$

With this definition, we have the averaged momentum equation for fluid 1

$$\theta_1 C_{1s}\mu_1\langle u_1\rangle = -\theta_1\nabla\langle p_1\rangle + F_{12}. \tag{23}$$

Similarly, the averaged momentum equation and the drag coefficient for fluid 2 can be written in the similar forms,

$$\theta_2 C_{2s}\mu_2\langle u_2\rangle = -\theta_2\nabla\langle p_2\rangle + F_{21}, \tag{24}$$

$$C_{2s} = \int_0^{\phi(x,t)} 32\bar{u}_2 P(\phi)\,d\phi \Big/ \int_0^{\phi(x,t)} \phi^2\bar{u}_2(x,t,\phi)P(\phi)\,d\phi, \tag{25}$$

with F_{21} defined as

$$F_{21} = [p_2(x,t,\phi(x,t)) - \langle p_2\rangle]\nabla\theta_2 = -[\langle p_2\rangle_I - \langle p_2\rangle]\nabla\theta_1, \tag{26}$$

where $\langle p_2\rangle_I = p_2(x,t,\phi(x,t))$ is the pressure of fluid 2 on the interface. Using (20) and (26), and noting that $p_1(x,t,\phi(x,t))$ and $p_2(x,t,\phi(x,t))$ are evaluated at the interface, we find

$$F_{12}(x,t) + F_{21}(x,t) = [\langle p_2\rangle(x,t) - \langle p_1\rangle(x,t) - 4\Gamma_{21}\cos\beta/\phi(x,t)]\nabla\theta_1 \tag{27}$$

after using (3).

Although in this paper we derived momentum equations (23) and (24) in the bundle-of-tubes model for a porous material, the functional forms of these momentum equations are quite general since similar equations are obtained in a more general treatment (see Part 2) after neglecting inertial terms.

If Darcy's law were assumed to be valid for each fluid phase, the force densities F_{12} and F_{21} have to vanish simultaneously implying $\langle p_2\rangle - \langle p_1\rangle = 4\Gamma_{21}\cos\beta/\phi(x,t)$. This is in agreement with the original concept of capillary pressure. According to Dahle et al. (2005), the quantity $4\Gamma_{21}\cos\beta/\phi(x,t)$ is a static part of the capillary pressure; and $\langle p_2\rangle - \langle p_1\rangle - 4\Gamma_{21}\cos\beta/\phi(x,t)$ is a dynamic part of the capillary pressure. Eqs. (23) and (24) show that the dynamic part of the capillary pressure not only affects the pressure difference but also presents itself as a term in the momentum equations.

These momentum equations together with the continuity equations

$$\frac{\partial\theta_i}{\partial t} + \nabla\cdot(\theta_i\langle u_i\rangle) = 0, \quad i = 1,2 \tag{28}$$

and the condition $\theta_1 + \theta_2 = \theta_p$, where θ_p is the porosity, form a closed system of equations provided closure relations for $\langle p_2\rangle - \langle p_1\rangle$ and F_{12} or F_{21} can be found. The closure relations for these quantities need to be expressed in terms of macroscopic quantities, such as average pressure of a phase and average velocities. For the simple bundle-of-tubes model, we obtain the closure relations using the analytical solution for flows in the tubes. For more complex pore morphologies, numerical results can be used for this purpose. However, even with the numerical results the averaging method does not give the functional forms for these closure quantities, but it does provide an explicit way to calculate the closure relationship using related quantities evaluated at the phase interfaces. This is a significant advantage of the averaging method. Although for a given practical problem if the flow details in the pores can be numerically calculated, the calculation of closure quantities is not practically useful to the problem itself. It is hoped that by explicitly calculating and studying the closure quantities in a few selected (simple) cases, one can obtain better understanding of the transport process and then formulate physically-based closure models for more complicated cases.

4. Properties of the closure relationships

In the bundle-of-tubes model, the key closure quantities, (i.e. the pressure difference, the drag coefficients, and the force densities F_{12} and F_{21}), can be calculated explicitly for a specified tube diameters distribution $P(\phi)$. In this section, we take this advantage and calculate the closure quantities. To facilitate the study of the relative magnitudes of the terms in the averaged equations, we non-dimensionalize the key terms. Length is non-dimensionalized by the characteristic length L of the capillary tube; force is non-dimensionalized by $\Gamma_{21}L$; and time is non-demensionalized by $\mu_1 L/\Gamma_{21}$. The length of the capillary tube, the viscosity of fluid 1 and the surface tension between the fluids are thereby set to unity. Table 1 shows the value of other quantities under this non-dimensionalization scheme. In the following calculations, we assume that the probability distribution for the tube diameters is uniform between the smallest pore size ϕ_s and the largest pore size ϕ_L as

$$P(\phi) = 1/(\phi_L - \phi_S). \tag{29}$$

4.1. Receding fluid with negligible viscosity

We first study a case in which the viscosity of fluid 2 is negligible and the pressures in both reservoirs are set to zero. This case resembles the scenario in which water replaces air in the capillary tubes at ambient conditions. Since the fluid 2 is inviscid, we have $p_2 = \langle p_2\rangle$ is a constant and $F_{21} = 0$. For simplicity, the constant pressure p_2 can be set to zero for incompressible fluid 2. Using (27) we have

$$F_{12} = -[\langle p_1\rangle(x,t) - \langle p_2\rangle + 4\Gamma_{21}\cos\beta/\phi(x,t)]\nabla\theta_1. \tag{30}$$

Although $\langle p_2\rangle$ is set to zero, we intentionally leave it in (30) to remind readers that only the pressure difference, not the absolute pressure, is important in this case of incompressible fluids in rigid tubes. The results shown in the figures of this subsection are obtained with pressure p_2 set to zero; therefore whenever the

Table 1
Parameters for bundle of tube models. The values of the dimensionless L, μ and Γ are equal to 1.

Parameter	Description	Value
L	Length or tube	1
μ_1	Viscosity of fluid 1	1
Γ	Surface tension	1
ϕ_s	Lower cut-off pore diameter	$10^{-8}L$
ϕ_L	Upper cut-off pore diameter	$10^{-3}L$
β	Contact angle	0 (rad)

pressure p_1 is mentioned in the text or in the figure, it should be understood as the pressure difference.

In this case, the interface location x in a specified tube can be solved from (5) and is proportional to the square root of time $\sqrt{t}$. As a consequence, at a given x and t, the pressure $p_1(x, t)$ for fluid 1 as calculated in (6) can be expressed in terms of the grouping $x/\sqrt{t}$. The same is true for the tube diameter ϕ solved from (5), the volume fraction θ_1 calculated using (9), the averaged pressure of fluid 1 $\langle p_1 \rangle$ calculated using (12), and the drag coefficient C_{1s} calculated using (22). The volume fraction, the saturation (defined as $S_1 = \theta_1/(\theta_1 + \theta_2)$), the drag coefficient, the average pressure, and the tube diameter can all be expressed as a single valued functions of $x/\sqrt{t}$ for different time t, as shown in Fig. 2. Similar profiles of S_1 vs. $x/\sqrt{t}$ are commonly reported for water imbibition in building materials (Hall et al., 1984; Lockington and Parlange, 2003; El Abd et al., 2005; Ridgway et al., 2006; Hall, 2007).

Fig. 2(c), the plot of $\langle p_1 \rangle$ vs. $x/\sqrt{t}$, suggests that the ensemble averaged pressure $\langle p_1 \rangle$ is not a monotonic function of $x/\sqrt{t}$. The response seen in Fig. 2(c) can be rationalized by referring to Fig. 1 and recalling that in this case both p_L and p_R are zero. For a specified time, ensemble averaging over the tubes at small values of x involves tubes (of various diameters) that all contain the invading fluid 1. Within each of these individual tubes the pressure decreases with increasing x. Thus the ensemble averaged pressure decreases with increasing x in this regime. However, when the ensemble average is performed at larger values of x, the tubes containing the invading fluid 1 are those tubes of larger diameter. This is a consequence of the fact that the velocity of invading fluid is slower in the smaller diameter tubes and thus at the specified time, and large enough values of x, the small diameter tubes are not yet filled by the invading fluid. At even larger values of x, only the very largest diameter tubes are filled with fluid 1. In such tubes the pressure drop due to friction with walls is relatively small compared to that in smaller tubes; and the pressure in forefront of the invading fluid is close to the pressure on the fluid interface, which is $-4\Gamma_{21}\cos\beta/\phi(x, t)$, an increasing function of x, because $\phi(x, t)$ increases with x. Only the filled tubes are counted in the ensemble phase averaging procedure used in the calculation of the average pressure of fluid 1. The resulting ensemble average then increases with x as shown in Fig. 2(c). In this case, the extended Darcy's law is invalid in the forefront of the invading fluid since it would predict negative velocities for fluid 1, if used. Difficulties associated with direct application of Darcy's law to two-phase flows in a porous medium have been recognized previously (Hall et al., 1996; Nordbotten et al., 2008). In an attempt to amend Darcy's law, a "macroscopic pressure" is sometimes defined as a linear combination of the spatial derivatives of the volume averaged pressure of various orders (Nordbotten et al., 2008). In the case of this bundle-of-tubes model, the ensemble phase average can be regarded as a volume average with the representative volume being a slab perpendicular to the tube direction with infinitesimal thickness in the direction of flow. For the case of inviscid fluid 2, the "macroscopic pressure" of the fluid vanishes, and flux of fluid 1 is then proportional the gradient of the "macroscopic pressure" of fluid 1 according to Eq. (33) of Nordbotten et al. (2008). Since the flux is positive in this example, this requires the gradient of the "macroscopic pressure" of fluid 1 to be negative. However, as shown in Fig. 2(c), the gradient of ensemble phase averaged pressure, which equals to the intrinsic volume averaged pressure, is positive. In other words, the gradient of the so-called "macroscopic pressure" and the gradient of the intrinsic volume averaged pressure have different signs; while the lowest order approximation to the "macroscopic pressure" is thought to be the intrinsic average pressure (Nordbotten et al., 2008).

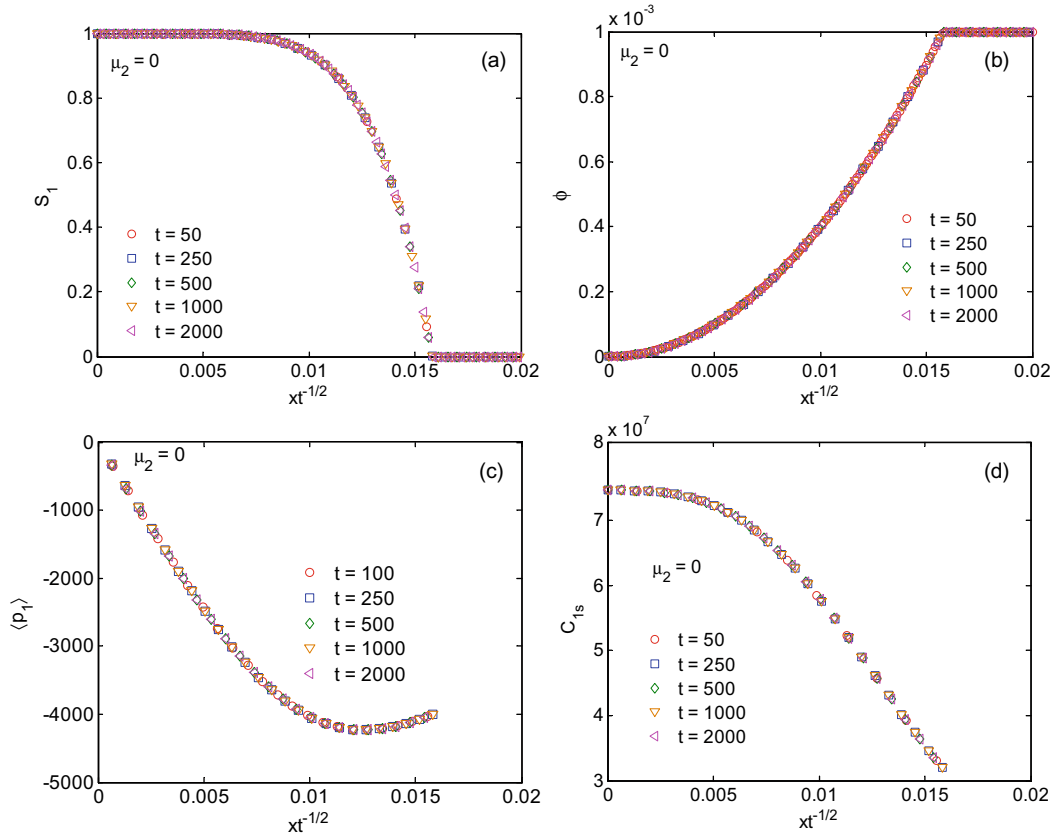

Fig. 2. The correlations of S_1 vs. $x/\sqrt{t}$ (a), ϕ vs.$x/\sqrt{t}$ (b), $\langle p_1 \rangle$ vs. $x/\sqrt{t}$ (c), and C_{1s} vs. $x/\sqrt{t}$ (d) at different imbibition times.

From (11) we find that saturation S_1 can be written as a single-valued function of diameter ϕ. As mentioned above the diameter $\phi(x,t)$ is a single-valued function of $x/\sqrt{t}$. Therefore the variable $x/\sqrt{t}$ can also be regarded as a single-valued function of the fluid 1 saturation S_1 in the region where the saturation $0 < S_1 < 1$, as shown in Fig. 2(a). In this region, the diameter $\phi(x,t)$, the averaged pressure $\langle p_1\rangle$ and the drag coefficient C_{1s} can be expressed as single-valued functions of the volume fraction θ_1, or saturation S_1. With these relations we can rewrite the momentum equation for fluid 1 as

$$\theta_1\langle u_1\rangle = -D_1(S_1)\nabla S_1, \quad 0 < S_1 < 1, \tag{31}$$

where

$$D_1(S_1) = \frac{\theta_p}{C_{1s}(S_1)\mu_1}\left[S_1\frac{d\langle p_1\rangle}{dS_1} + \langle p_1\rangle(S_1) - \langle p_2\rangle + 4\Gamma_{21}\cos\beta/\phi(S_1)\right]. \tag{32}$$

In this way the volume flux $\theta_1\langle u_1\rangle$ per unit cross section area can be expressed in a form similar to Fick's law of diffusion with a saturation-dependent diffusion coefficient $D_1(S_1)$. This imbibition flow can be described as a diffusion process because the averaged pressure difference $\langle p_1\rangle(S_1) - \langle p_2\rangle$, the surface tension term $4\Gamma_{21}\cos\beta/\phi$, and the drag coefficient C_{1s} depend only on the saturation. This explains the success of the diffusion approach in modeling imbibition of liquids when gas viscosity is negligible (Washburn, 1921). However, this condition is only satisfied in the cases where the viscosity of the receding fluid is negligible and in the region where S_1 is less than one. In cases where $S_1 = 1$, as shown in Fig. 2(a), we have $\nabla S_1 = 0$, while the fluid flux $\theta_1\langle u_1\rangle > 0$; therefore (31) is incorrect. In this region, $F_{12} = 0$ according to (20), and thus the fluid is purely driven by the pressure gradient term in the momentum equation (23). Indeed, in this region, the average pressure $\langle p_1\rangle$ decreases linearly with x as shown in Fig. 2(c) while the saturation remains constant. The derivative $d\langle p_1\rangle/dS_1$ then becomes undefined and the diffusivity defined by (32) becomes infinity as shown in Fig. 3(a). This explains that many reported experimental values for D_1 increase significantly (as much as 10^4 times), as the saturation approaches unity (Meyer and Warrick, 1990; El Abd et al., 2005). The fact that the diffusivity becomes undefined in the region of full saturation, highlights a limitation of the diffusion approach of describing fluid imbibition processes in porous materials.

This example demonstrates the importance of the additional force density term, F_{12}, in the ensemble averaged momentum equation (23). The force density F_{12} can be calculated from the pressure difference $\langle p_1\rangle_I - \langle p_1\rangle$ by using (20). In Fig. 3(b)–(d), the relation between the pressure difference $\langle p_1\rangle_I - \langle p_1\rangle$, the surface tension, and the drag coefficient are plotted as functions of the saturation S_1 of fluid 1. In this case of negligible viscosity of fluid 2, all of these closure quantities for fluid 1 are single-valued functions of S_1.

4.2. Receding fluid with finite viscosity

In this subsection we study a case in which the pressure difference between reservoirs is still zero, but viscosity μ_2 of fluid 2 is not negligible. The viscosity ratio, μ_2/μ_1 between fluid 2 and fluid 1 is set to be in a range from 0.01 to 1. In this case, surface tension generates the pressure gradient needed to drive fluid 2, hence $p_2 > 0$ and $\langle p_2\rangle > 0$. Fig. 4(a) plots the average pressures as a function of x at different time t. We note that there are kinks in the curves for the average pressure $\langle p_2\rangle$ of fluid 2. The curve for the average pressure $\langle p_1\rangle$ stops at the x-coordinate of the kink point for the corresponding average pressure $\langle p_2\rangle$. This kink point is the deepest penetration for the invading fluid at the specified time. After that point, the fluid 1 is not present and the average pressure

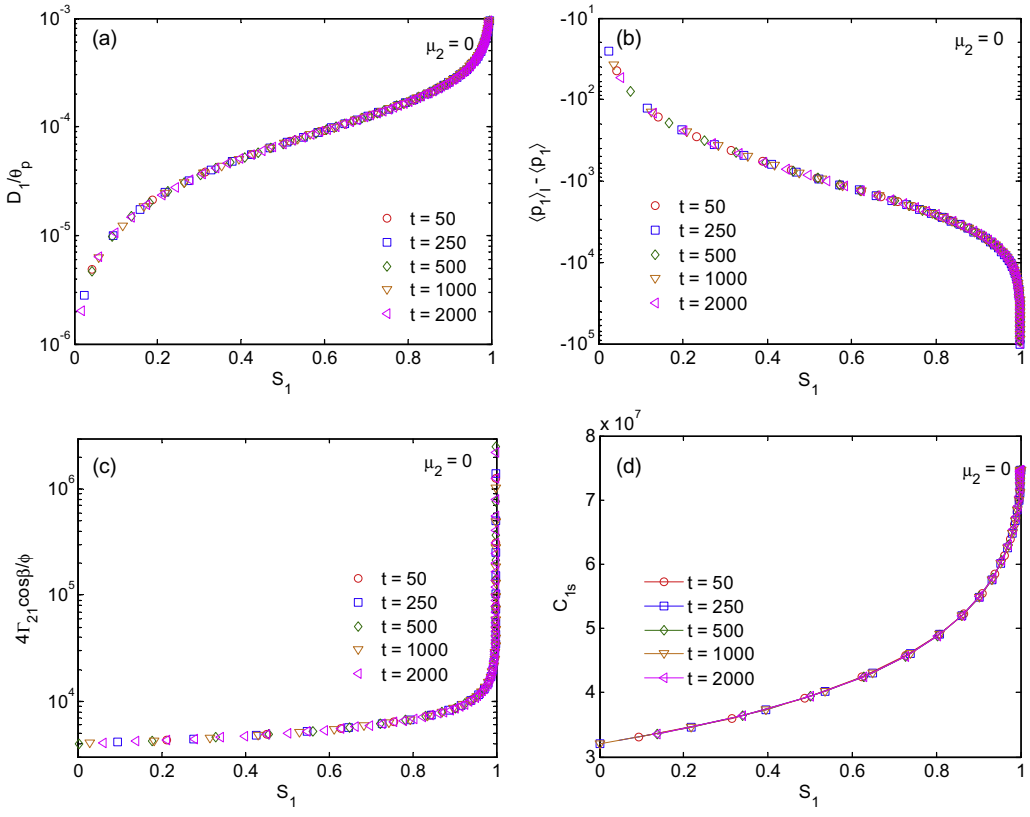

Fig. 3. The correlations of D_1/θ_p vs. S_1 (a), $\langle p_1\rangle_I - \langle p_1\rangle$ vs. S_1 (b), $4\Gamma_{21}\cos\beta/\phi$ vs. S_1 (c), and C_{1s} vs. S_1 (d).

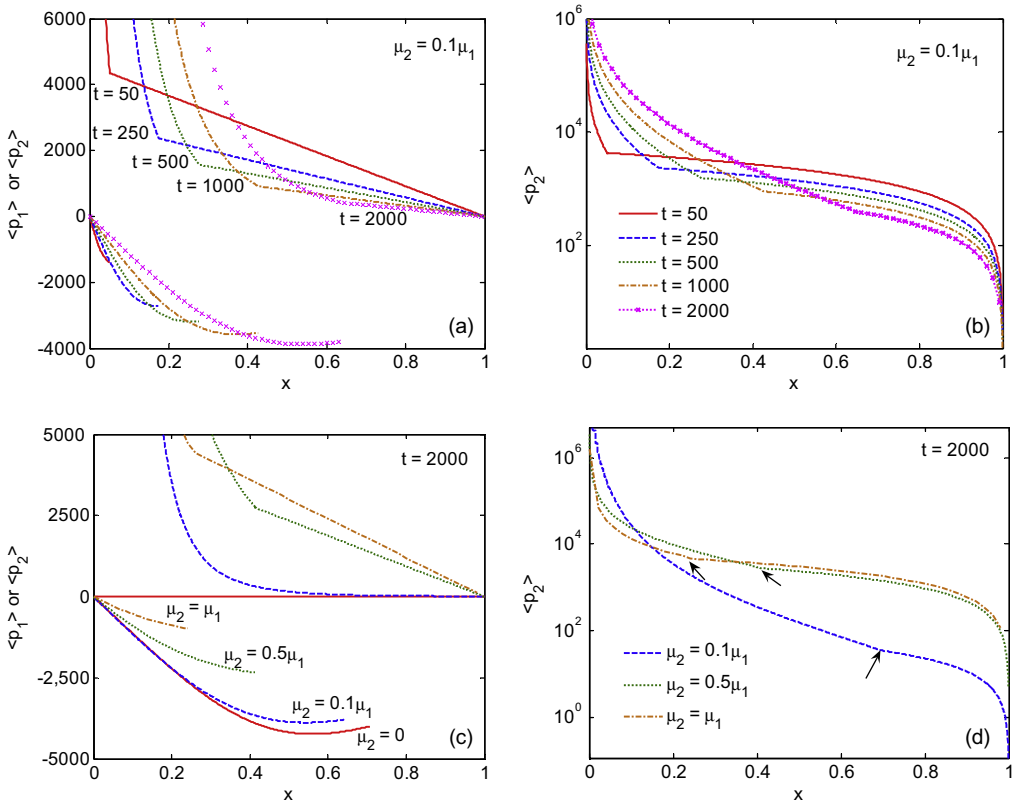

Fig. 4. The profiles of the average pressures of two phases ($\langle p_1\rangle$or $\langle p_2\rangle$) vs. x without the external pressure difference, (a and b) imbibition time effect, and (c and d) viscosity ratio effect. Arrows in the plot indicate the kinks.

of fluid 1 is undefined. After the kink, the average pressure $\langle p_2\rangle$ varies linearly with x. To explain this phenomenon, we note that similar to Eq. (19), we have

$$\theta_2\nabla\langle p_2\rangle = \theta_2\langle\nabla p_2\rangle + [\langle p_2\rangle_I - \langle p_2\rangle]\nabla\theta_2, \tag{33}$$

where $\langle p_2\rangle_I$ is the pressure of fluid 2 at the phase interface. When x is larger than the x-coordinate of the kink point, all the tubes are filled with fluid 2, and $\nabla\theta_2 = 0$. In each tube, according to (2), the pressure gradient ∇p_2 is independent of x, and so is its average $\langle\nabla p_2\rangle$. The gradient of the averaged pressure calculated from (33) is then independent of x; and $\langle p_2\rangle$ varies linearly with x as shown in Fig. 4(a). In the coexisting region for both phases, the average pressures are highly nonlinear. Fig. 4(b) shows that the magnitude of $\langle p_2\rangle$ is much larger than that of $\langle p_1\rangle$ because fluid 2 preferentially occupies small tubes. Fig. 4(c) and (d) shows the effect of viscosity ratio on the average pressure profiles for the two phases at a specified time. As the viscosity ratio increases, the non-monotonic behavior of $\langle p_1\rangle$ disappears.

Fig. 5(a) shows that the saturation is not a single valued function $x/\sqrt{t}$ when the viscosity ratio of two phases is non-zero. Fig. 5(b) and (c) shows that the pressure difference $\langle p_1\rangle_I - \langle p_1\rangle$ of fluid 1 at the interface and the pressure difference $\langle p_2\rangle - \langle p_1\rangle$ between two phases depend not only on the saturation but also on time t. Fig. 5(d) shows the drag coefficient C_{1s} as a function of the saturation S_1 at different times. This coefficient is a weak function of time t, as no significant change of C_{1s} is observed by changing the time t from 50 to 2000.

These results imply that a parameter in addition to the saturation S_1 is needed to uniquely determine the closure relationships. In introducing the concept of dynamic capillary pressure, Hassanizadeh and Gray (1993), assumed that the dynamic part of the capillary pressure was proportional to the local time derivative $\partial S_1/\partial t$. This idea can be generalized to model the closure quantities as nonlinear functions of the saturation S_1 and its local time derivative $\partial S_1/\partial t$. In the bundle-of-tubes model, for a given pair of S_1 and $\partial S_1/\partial t$, there is a unique corresponding pair of x and t. With a uniform distribution of diameters (given by the probability distribution) between ϕ_S and ϕ_L, the required relationship can be found as follows. By differentiating (5) and (11) with respect to t, and then eliminating $\partial\phi/\partial t$, from the resulting relations we find

$$\frac{1}{t} = \frac{(\phi_L^3 - \phi_S^3)(2\phi\Delta p + 4\Gamma_{21}\cos\beta)}{3\phi^3(\phi\Delta p + 4\Gamma_{21}\cos\beta)}\frac{\partial S_1}{\partial t}. \tag{34}$$

Using (11) the diameter ϕ can be expressed in terms of saturation S_1 as

$$\phi(S_1) = \sqrt[3]{\phi_L^3 - S_1(\phi_L^3 - \phi_S^3)}. \tag{35}$$

With (34) and (35), the time t can then be expressed as a function of saturation S_1 and its local time derivative $\partial S_1/\partial t$. Using (5) and (35), position x can also be expressed as a function of the saturation S_1 and $\partial S_1/\partial t$. The closure quantities calculated at (x, t) can then be expressed as functions of these two primary variables, S_1 and $\partial S_1/\partial t$. These functions are shown in Fig. 6. For a fixed $\partial S_1/\partial t$, the relation between $\langle p_1\rangle_I - \langle p_1\rangle$ and S_1 is non-monotonic as shown in Fig. 6(a). At a small $\partial S_1/\partial t$, this non-monotonic behavior is more pronounced. For a given $\partial S_1/\partial t$, initially the pressure difference $\langle p_1\rangle_I - \langle p_1\rangle$ decreases with the saturation S_1, but as the saturation approaches unity, the pressure difference starts to increase. This behavior may seem to be in contradiction to the pressure difference plotted in Fig. 5(b). To explain this apparent contradiction, one needs to recall that these two figures are obtained under different conditions. Fig. 5(b) is obtained at a constant time whereas Fig. 6(a) is obtained at a fixed $\partial S_1/\partial t$ (= $-\partial S_2/\partial t$). According to (4),

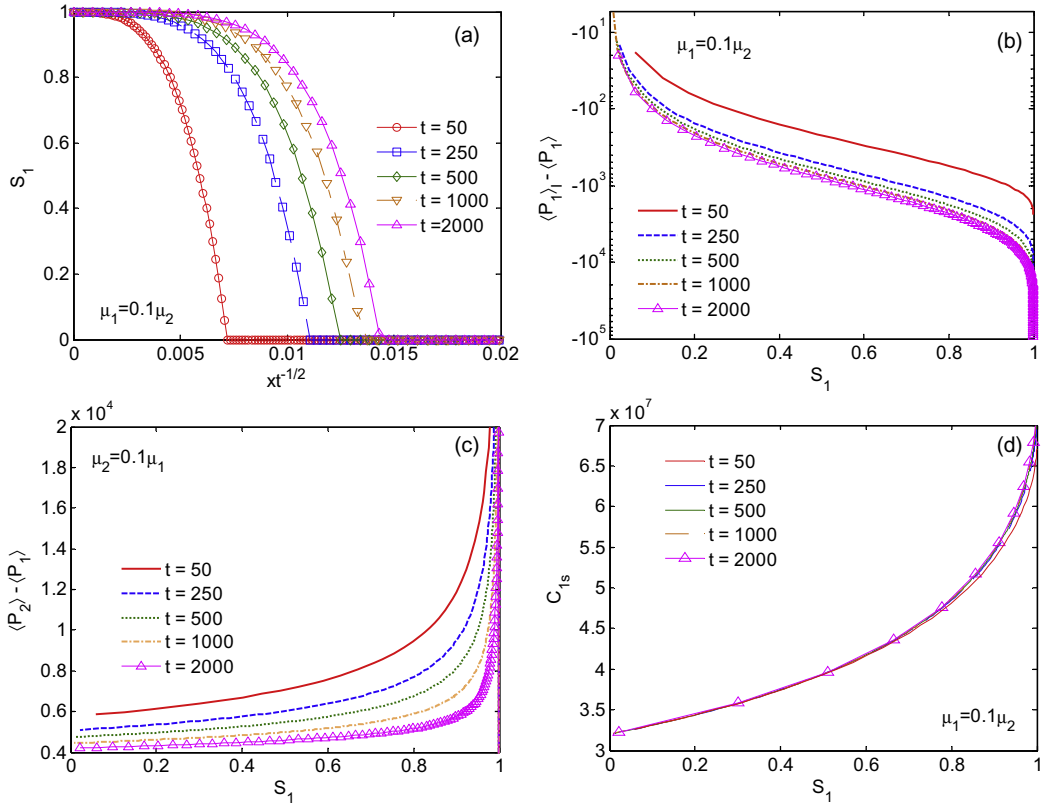

Fig. 5. The correlations of S_1 vs. $x/\sqrt{t}$ (a), $\langle p_1\rangle_I - \langle p_1\rangle$ vs. S_1 (b), $\langle p_2\rangle - \langle p_1\rangle$ vs. S_1, and C_{1s} vs. S_1 (d).

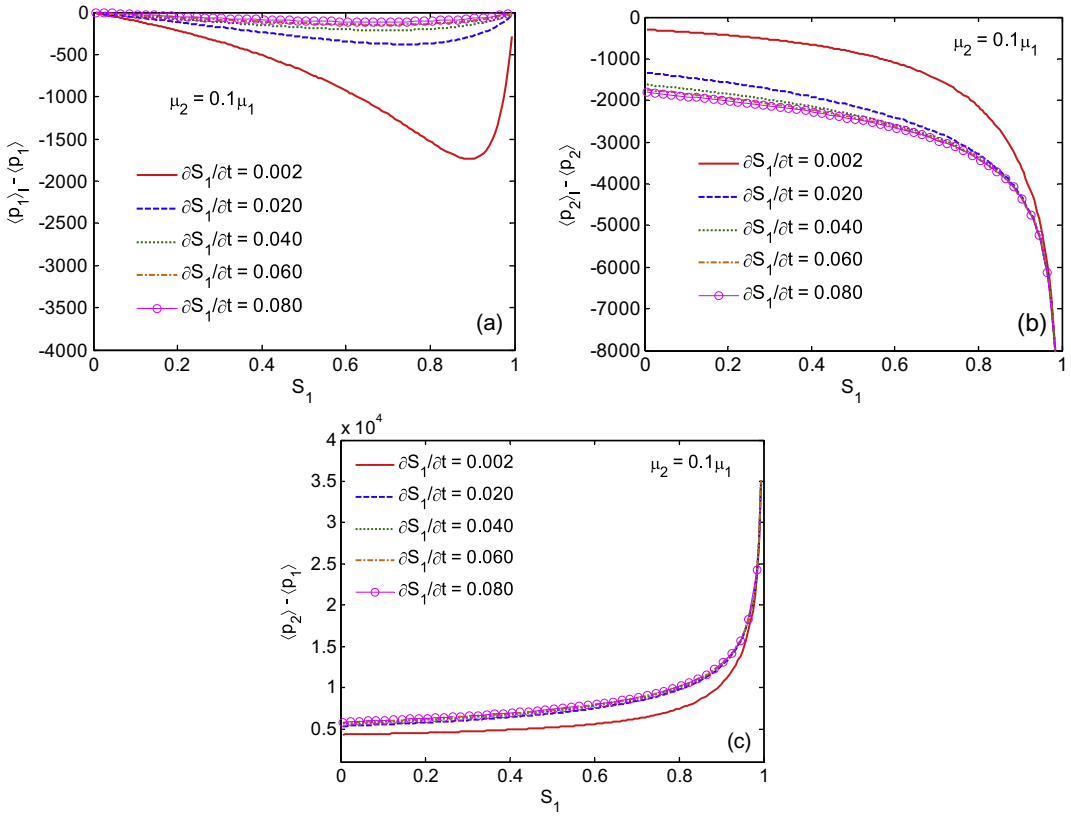

Fig. 6. The effect of $\partial S_2/\partial t$ on the profile of $\langle p_1\rangle_I - \langle p_1\rangle$ vs. S_1 (a), $\langle p_2\rangle_I - \langle p_2\rangle$ vs. S_1 (b), and $\langle p_2\rangle - \langle p_1\rangle$ vs. S_1 (c).

flow velocity increases with the tube diameter and the invading fluid occupies the large tubes first. As the saturation S_1 approaches unity and saturation S_2 approaches zero, the diameters of the tubes containing fluid 2 (and thus the velocity of fluid 2) become small. Thus, the second term in the continuity equation for fluid 2 becomes small and negligible

$$\frac{\partial S_2}{\partial t} + S_2 \nabla \cdot \langle u_2 \rangle + \langle u_2 \rangle \cdot \nabla S_2 = 0. \tag{36}$$

The pressure difference $\langle p_1 \rangle_I - \langle p_1 \rangle$ in Fig. 6(a) is obtained with fixed $\partial S_2/\partial t$, thus as velocity $\langle u_2 \rangle$ decreases, the magnitude of $|\nabla S_2|$ increases. Since the change in the saturation is caused by moving across the fluid interfaces, the large saturation gradient indicates a point close to fluid interfaces. Therefore the pressure difference $\langle p_1 \rangle_I - \langle p_1 \rangle$ in Fig. 6(a) is calculated with the average pressure $\langle p_1 \rangle$ evaluated at a point close to the interface; and thus the pressure difference is of lower magnitude as seen in Fig. 6(a). The same is true for the pressure difference $\langle p_2 \rangle_I - \langle p_2 \rangle$ of fluid 2, however, it is not shown in Fig. 6(b), because the minimum for this pressure difference occurs at saturation $S_2 \approx 10^{-8}$ according to the assumed probability distribution (29) of the tube diameters. Fig. 6(c) shows the average pressure difference between two phases as a function of S_1 and $\partial S_1/\partial t$.

Similar to the observation in Fig. 5(d), Fig. 7(a) and (b) shows that C_{1S} and C_{2S} are functions of S_1 but are almost independent of $\partial S_2/\partial t$. This explains why the permeability (the inverse of these drag coefficients) is often reported not to be rate dependent, although it is often reported to be dependent on the degree of saturation (Brooks and Corey, 1964; Braun et al., 2005).

In this simple bundle-of-tubes model, the static part of the capillary pressure (Dahle et al., 2005), $4\Gamma_{21}\cos\beta/\phi$, is only a function of the saturation. This is because the tube diameter ϕ is only a function of the saturation as shown in (11) and (35). In Fig. 8, we display the dynamic part of the capillary pressure $\langle p_2 \rangle - \langle p_1 \rangle - 4\Gamma\cos\beta/\phi$. Initially it was thought (Hassanizadeh and Gray, 1993) that the dynamic part of the capillary pressure was proportional to $\partial S_1/\partial t$. Later Dahle et al. (2005) found that when $\partial S_1/\partial t = 0$, the dynamic part of the capillary pressure was not zero. They then modified the dynamic capillary pressure to contain two terms. The first term is a function of the saturation S_1 only. The second term is proportional to $\partial S_1/\partial t$ with a coefficient depending on S_1. For cases with $\mu_2 \ll \mu_1$, $\langle p_2 \rangle = 0$ and $\langle p_1 \rangle$ is a function of the saturation, as explained above. The dynamic part of the capillary pressure is then a function of saturation only and is independent of $\partial S_1/\partial t$ as shown in Fig. 8. However, for the cases where μ_2 is not negligible, our results show that the capillary pressure depends on $\partial S_1/\partial t$ in a non-linear manner. The strongest response occurs at small values of $\partial S_1/\partial t$. As $\partial S_1/\partial t$ increases, the value of $\langle p_2 \rangle - \langle p_1 \rangle - 4\Gamma\cos\beta/\phi$ approaches a constant value.

To study the effects of the viscosity ratio, we fix the value of S_1 at 0.5 and then plot $\langle p_2 \rangle - \langle p_1 \rangle - 4\Gamma\cos\beta/\phi$ as a function of $\partial S_1/\partial t$ in Fig. 9. The dynamic pressure is sensitive to $\partial S_1/\partial t$ for a small $\partial S_1/\partial t$ and approaches a constant for a large $\partial S_1/\partial t$. When the viscosity ratio

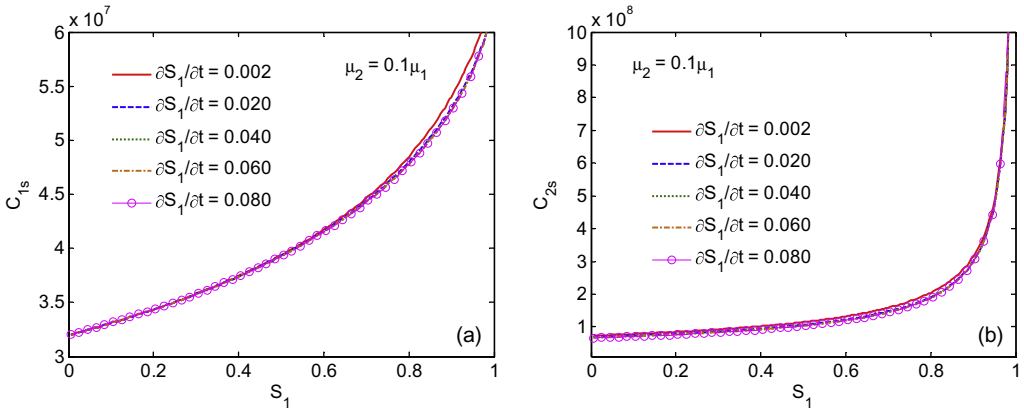

Fig. 7. The effect of $\partial S_2/\partial t$ on the profile of C_{1s} vs. S_1 (a) and C_{2s} vs. S_1 (b).

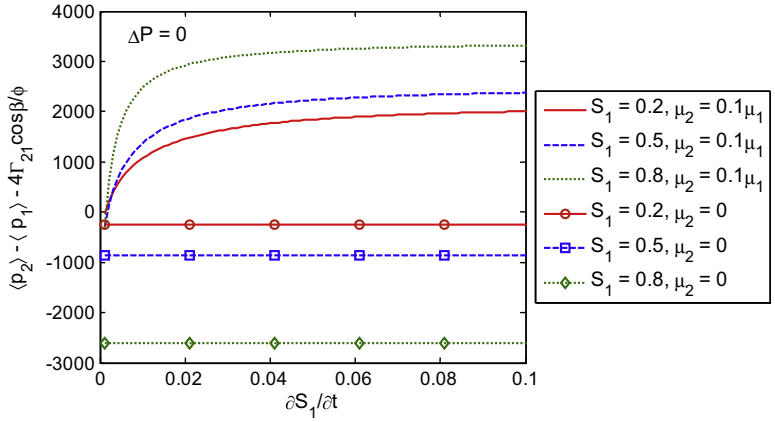

Fig. 8. The correlation between $\langle p_2 \rangle - \langle p_1 \rangle - 4\Gamma\cos\beta/\phi$ and $\partial S_1/\partial t$ at targeted S_1 and $\Delta P = 0$.

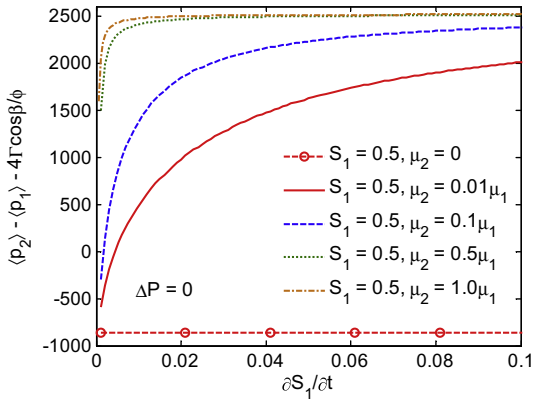

Fig. 9. The correlation between $\langle p_2\rangle - \langle p_1\rangle - 4\Gamma\cos\beta/\phi$ and $\partial S_1/\partial t$ at different viscosity at $S_1 = 0.5$.

between the receding and the invading fluids decreases, the saturation rate dependent region of $\langle p_2\rangle - \langle p_1\rangle - 4\Gamma\cos\beta/\phi$ expands.

4.3. Effects of reservoir pressure difference

To examine the effects of the pressure difference in the reservoir, we recalculate all the quantities in Figs. 6–8 with $\Delta P = 10^4$ and plot the results in Fig. 10.

With the positive pressure difference Δp, there is a larger velocity increase in large tubes than that in small tubes as one would expect. The increase in the penetration of fluid 1 is also more significant in larger tubes than that in small tubes, resulting in a larger spread in the co-existence regions of fluids. This leads to an increase in the average distance from a point x (where the average pressure is evaluated) to the interface where $\langle p_1\rangle_I$ and $\langle p_2\rangle_I$ are evaluated. This results in more significant pressure differences $\langle p_1\rangle_I - \langle p_1\rangle$ and $\langle p_2\rangle_I - \langle p_2\rangle$ in Fig. 10(a) and (b) than the pressure

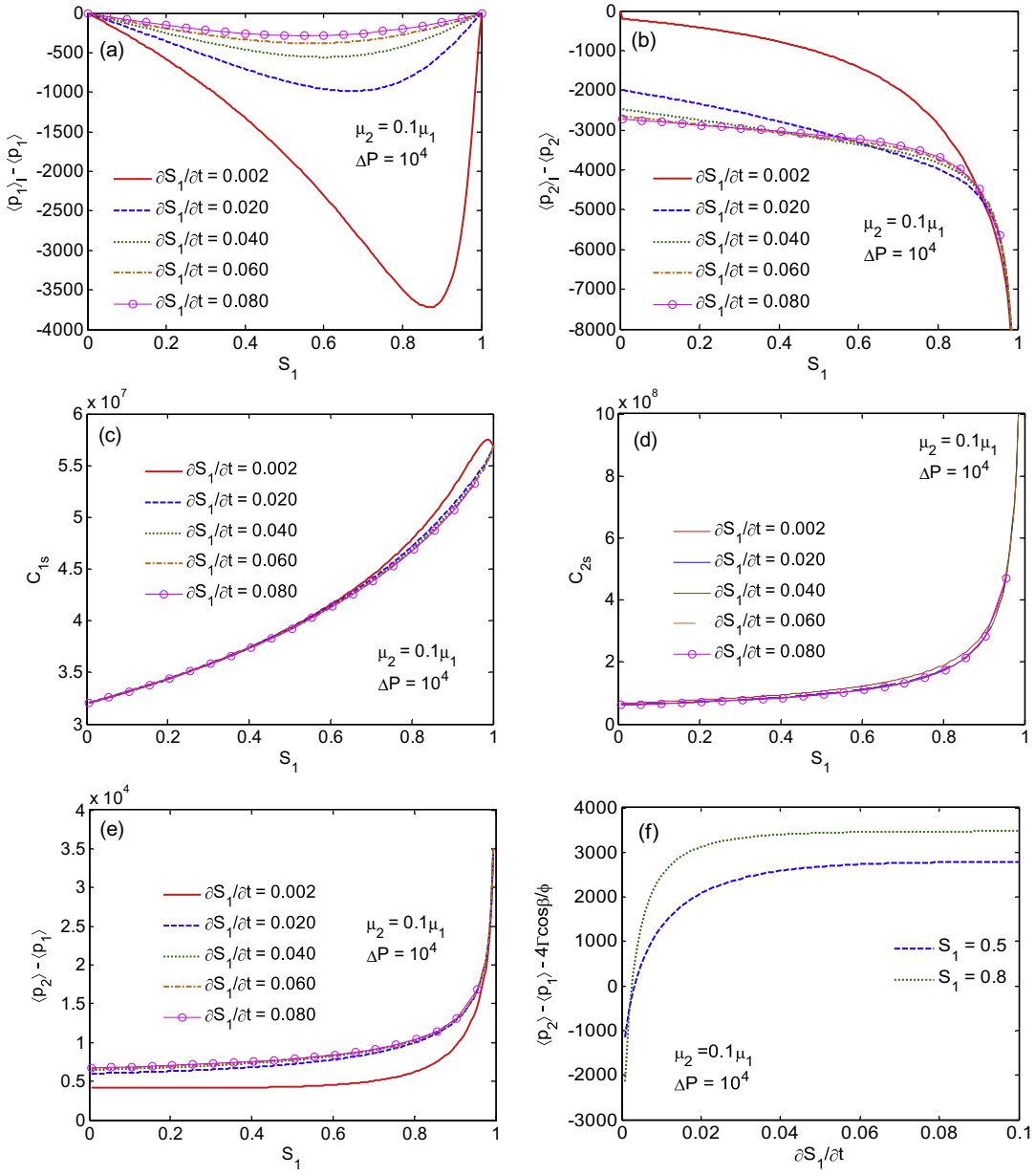

Fig. 10. Plots $\langle p_1\rangle_I - \langle p_1\rangle$ vs. S_1 (a), $\langle p_2\rangle_I - \langle p_2\rangle$ vs. S_1 (b), C_{1s} vs. S_1 (c), C_{2s} vs. S_1 (d), and $\langle p_2\rangle - \langle p_1\rangle$ vs. S_1 (e) at different $\partial S_1/\partial t$ with $\Delta P = 10^4$. The correlation between $\langle p_2\rangle - \langle p_1\rangle - 4\Gamma\cos\beta/\phi$ and $\partial S_1/\partial t$ at different S_1 is plotted in (f).

differences in Fig. 6 (a) and (b). The pressure difference $\langle p_2\rangle - \langle p_1\rangle$ between phases shown in Fig. 10(e), however, is almost the same as in Fig. 6(c), because they are not directly related to external pressures. The drag coefficients of C_{S1} and C_{S2} in Fig. 10(c) and (d) are almost the same as those in Fig. 7(a) and (b). Again, the behavior of dynamic part of the capillary pressure shows a nonlinear dependence on $\partial S_1/\partial t$ in Fig. 10(f).

The average pressure difference $\langle p_2\rangle - \langle p_1\rangle$ between phases is commonly called the capillary pressure implying an assumption that it is a result of surface tension. We now calculate a case without the surface tension. We keep all other parameters the same as in the last case except we set $\Gamma = 0$. The results of $\langle p_1\rangle_I - \langle p_1\rangle$ are plotted in Fig. 11(a). The curves behave similarly to the case plotted in Fig. 6(a), but with smaller magnitude due to the zero surface tension. The results of $\langle p_2\rangle_I - \langle p_2\rangle$ are plotted in Fig. 11(b). The pressure difference $\langle p_2\rangle_I - \langle p_2\rangle$ approaches zero as the saturation S_1 approaches unity. This property is also true for Fig. 6(b) but was not shown in the figure since the minimum value of the pressure difference occurs at the saturation S_1 too close to unity. As shown in Fig. 11(c), the average pressure difference $\langle p_2\rangle - \langle p_1\rangle$ is not zero. In this case, this difference in average pressures is caused by the viscosity difference between the fluids, not by surface tension. If the viscosity is the same as the cases studied by Dahle et al. (2005), then the average pressures of the two phases are in fact the same. In other words, not only the surface tension, but also viscosity difference contributes to the pressure difference, or the "capillary pressure".

5. Conclusions

In this paper, an ensemble phase averaging technique for continuous multi-material interactions is applied to derive averaged equations for multiphase flows in porous media. The ensemble averaged equations are found to have terms in addition to those commonly used in Darcy's law. Based on the bundle-of-tubes model, we studied properties of these additional terms. We find these

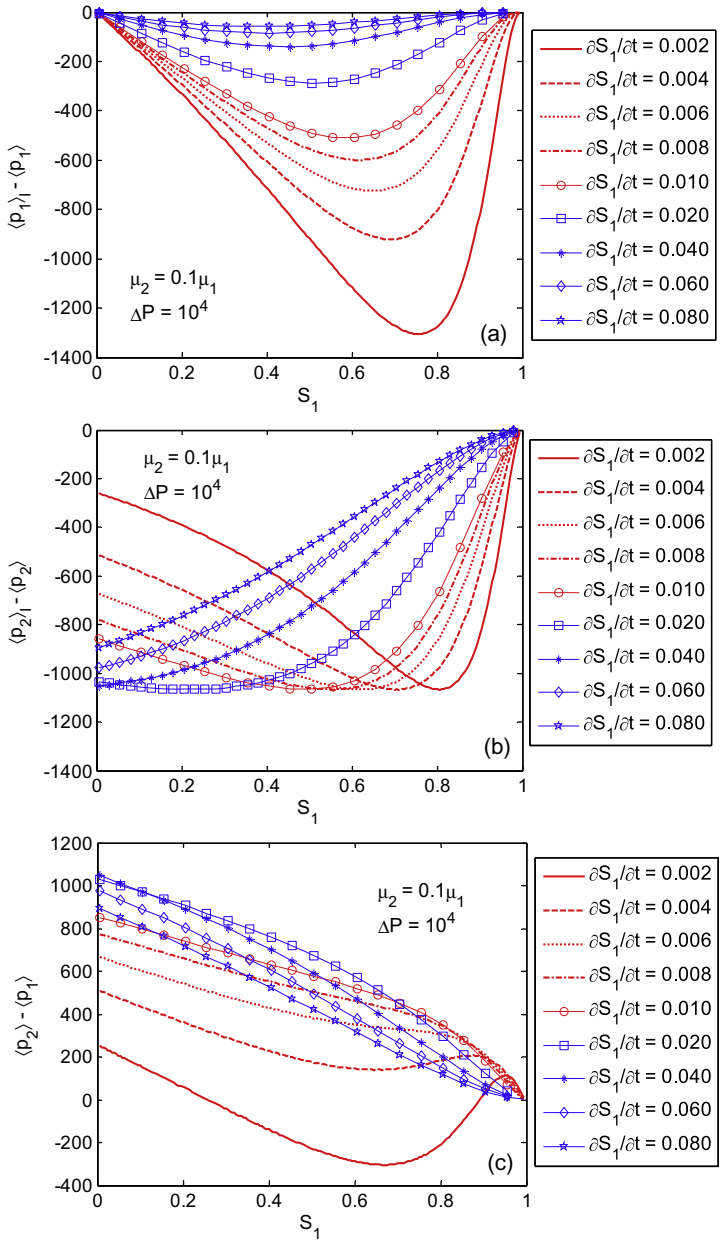

Fig. 11. Plots $\langle p_1\rangle_I - \langle p_1\rangle$, $\langle p_2\rangle_I - \langle p_2\rangle$, and $\langle p_2\rangle - \langle p_1\rangle$ vs. S_1 at different $\partial S_1/\partial t$in the case of $\Gamma_{21} = 0$.

new terms correct many deficiencies in models based on the straightforward extensions of Darcy's law. We also studied the relations between these new terms and several recent models for two-phase flows in porous media.

Closure relationships were derived for the simple bundle-of-tubes model. The closure can be written as functions of saturation and the local time derivative of the saturation. The drag coefficients were found to be almost independent of the local time derivative of the saturation. Despite the name "capillary pressure", the difference in the average pressures of two fluids is not necessary related to surface tension effects. Without surface tension, the average pressures of the two phases are not necessary the same. If the pressure difference can be decomposed into a static part, representing surface tension effects, and a dynamic part, as suggested by Dahle et al. (2005), then the dynamic part of the capillary pressure not only affects the pressure difference, but also appears as terms in the averaged momentum equations.

Although it is commonly assumed that a fluid imbibition process can be modeled as a diffusion process, in the example we show that this is not generally true. It is not necessary that the velocity of the invading fluid decreases as $1/\sqrt{t}$. If the fluid being displaced is more viscous than the invading fluid, the velocity can even increase with time as fluid in the pores is replaced by the less viscous invading fluid.

The results and conclusions obtained in this paper are based on the simple geometry of the bundle-of-tubes model. Although we have reason to believe that the closure relations obtained here share many common features and trends in more complicated systems, more work is needed before these conclusions can be generalized.

Acknowledgements

This work is funded by the United States Department of Homeland Security as part of a project to better understand the interaction between toxic chemicals and porous environmental substrates. We also wish to thank Dr. David Janecky at Los Alamos National Laboratory for his support in executing this work.

References

Alava, M., Dube, M., Rost, M., 2004. Imbibition in disordered media. Adv. Phys. 53, 83–175.

Beliaev, A.Y., Hassanizadeh, S.M., 2001. A theoretical model of hysteresis and dynamic effects in the capillary relation for two-phase flow in porous media. Transport Porous Med. 43, 487–510.

Braun, C., Helmig, R., Manthey, S., 2005. Macro-scale effective constitutive relationships for two-phase flow processes in heterogeneous porous media with emphasis on the relative permeability-saturation relationship. J. Contam. Hydrol. 76, 47–85.

Brooks, R.H., Corey, A.T., 1964. Hydraulic properties of porous media. In: Corey, A.T., Dils, R.E., Yevdjevich, V.M. (Eds.), Hydrology Papers. Colorado State University, Fort Collins.

Culligan, K.A., Wildenschild, D., Christensen, B.S.B., Gray, W.G., Rivers, M.L., Tompson, A.F.B., 2004. Interfacial area measurements for unsaturated flow through a porous medium, Water Resour. Res., 40, W12413.

Czachor, H., 2007. Applicability of the Washburn theory for determining the wetting angle of soils. Hydrol. Process. 21, 2239–2247.

Dahle, H.K., Celia, M.A., Hassanizadeh, S.M., 2005. Bundle-of-tubes model for calculating dynamic effects in the capillary-pressure–saturation relationship. Transport Porous Med. 58, 5–22.

DiCarlo, D.A., 2007. Capillary pressure overshoot as a function of imbibition flux and initial water content. Water Resour. Res. 43, W08402.

El Abd, A.E.G., Czachor, A., Milczarek, J.J., Pogorzelski, J., 2005. Neutron radiography studies of water migration in construction porous materials. IEEE Trans. Nucl. Sci. 52, 299–304.

Faybishenko, B., 2004. Nonlinear dynamics in flow through unsaturated fractured porous media: status and perspectives. Rev. Geophys. 42, 30.

Gray, W.G., Hassanizadeh, S.M., 1991. Unsaturated flow theory including interfacial phenomena. Water Resour. Res. 27, 1855–1863.

Gray, W.G., Tompson, A.F.B., Soll, W.E., 2002. Closure conditions for two-fluid flow in porous media. Transport Porous Med. 47, 29–65.

Gummerson, R.J., Hall, C., Hoff, W.D., Hawkes, R., Holland, G.N., Moore, W.S., 1979. Unsaturated water flow with porous materials observed by NMR imaging. Nature 281, 56–57.

Hall, C., 2007. Anomalous diffusion in unsaturated flow: fact or fiction? Cement Concrete Res. 37, 378–385.

Hall, C., Hoff, W.D., Nixon, M.R., 1984. Water-movement in porous building-materials. 6. Evaporation and drying in brick and block materials. Build. Environ. 19, 13–20.

Hall, C., Green, K., Hoff, W.D., Wilson, M.A., 1996. A sharp wet front analysis of capillary absorption into *n*-layer composite. J. Phys. 29, 2947–2950.

Hassanizadeh, S.M., Gray, W.G., 1993a. Thermodynamic basis of capillary-pressure in porous-media. Water Resour. Res. 29, 3389–3405.

Hassanizadeh, S.M., Gray, W.G., 1993b. Toward an improved description of the physics of two-phase flow. Adv. Water Resour. 16, 53–67.

Hilfer, R., 2006. Macroscopic capillarity without a constitutive capillary pressure function. Physica A 371, 209–225.

Hillel, D., 1980. Fundamentals of Soil Physics. Academic Press, New York.

Ianson, S.J., Hoff, W.D., 1986. Water-movement in porous building-materials. 8. Effects of evaporative drying on height of capillary rise equilibrium in walls. Build. Environ. 21, 195–200.

Le Guen, S.S., Kovscek, A.R., 2006. Nonequilibrium effects during spontaneous imbibition. Transport Porous Med. 63, 127–146.

Leverett, M.C., 1941. Capillary behavior in porous solids. Am. Inst. Mining Metall. Eng. – Petrol. Dev. Technol. 142, 152–168.

Liu, J.Y., 1991. Drying of porous materials in a medium with variable potentials. J. Heat Transfer Trans. ASME 113, 757–762.

Lockington, D.A., Parlange, J.Y., 2003. Anomalous water absorption in porous materials. J. Phys. D 36, 760–767.

Manthey, S., Hassanizadeh, S.M., Helmig, R., 2005. Macro-scale dynamic effects in homogeneous and heterogeneous porous media. Transport Porous Med. 58, 121–145.

Meyer, J.J., Warrick, A.W., 1990. Analytical expression for soil water diffusivity derived. Soil Sci. Soc. Am. J. 56, 1547–1552.

Moseley, M.A., Dhir, V.K., 1996. Capillary pressure–saturation relations in porous media including the effect of wettability. J. Hydrol. 178, 33–53.

Nordbotten, J.M., Celia, M.A., Dahle, H.K., Hassanizadeh, S.M., 2008. On the definition of macroscale pressure for multiphase flow in porous media. Water Resour. Res. 44, 06S02.

Pachepsky, Y.A., Timlin, D.J., Rawsls, W.J., 2003. Generalized Richards' equation to simulate water transport in unsaturated soils. J. Hydrol. 279, 290.

Prat, M., 1995. Isothermal drying of non-hygroscopic capillary-porous materials as an invasion percolation process. Int. J. Multiphase Flow 21, 875–892.

Richards, L.A., 1931. Capillary conduction of liquids through porous mediums. Physics 1, 318–333.

Ridgway, C.J., Gane, P.A.C., El Abd, A.E.G., Czachor, A., 2006. Water absorption into construction materials: comparison of neutron radiography data with network absorption models. Transport Porous Med. 63, 503–525.

Scheidegger, A.E., 1974. The Physics of Flow through Porous Media. University of Toronto, Ont. Canada, Toronto.

Shiozawa, S., Fujimaki, H., 2004. Unexpected water content profiles under flux-limited one-dimensional downward infiltration in initially dry granular media. Water Resour. Res. 40, W07404.

Tsakiroglou, C.D., Theodoropoulou, M.A., Karoutsos, V., 2003. Nonequilibrium capillary pressure and relative permeability curves of porous media. AIChE J. 49, 2472–2486.

Washburn, E.W., 1921. The dynamics of capillary flow. Phys. Rev. 17, 10.

Zhang, D.Z., 2009. Ensemble phase averaged equations for multiphase flows in porous media. Part 2: A general theory. Int. J. Multiphase Flow 35, 640–649.

Zhang, D.Z., Prosperetti, A., 1994. Averaged equations for inviscid disperse two-phase flow. J. Fluid Mech. 267, 185–219.

Zhang, D.Z., Prosperetti, A., 1997. Momentum and energy equations for disperse two-phase flows and their closure for dilute suspensions. Int. J. Multiphase Flow 23, 425–453.

Zhang, D.Z., VanderHeyden, W.B., Zou, Q., Padial-Collins, N.T., 2007. Pressure calculations in disperse and continuous multiphase flows. Int. J. Multiphase Flow 33, 86–100.